

Cite this: *Mater. Adv.*, 2020,
1, 2717Received 3rd August 2020,
Accepted 6th October 2020

DOI: 10.1039/d0ma00563k

rsc.li/materials-advances

Oxygen defective cerium oxide $\text{CeO}_{2-\delta}$ exhibits a non-classical giant electromechanical response that is superior to that of lead-based electrostrictors. In this work, we report the key-role of acceptor dopants, with different size and valence (Mg^{2+} , Sc^{3+} , Gd^{3+} , and La^{3+}), on polycrystalline bulk ceria. Different dopants tune the electrostrictive properties by changing the electrosteric dopant–defect interactions. We find two distinct electromechanical behaviors: when the interaction is weak (dopant–vacancy binding energy ≤ 0.3 eV), electrostriction displays a high coefficient (M_{33}), up to 10^{-17} (m V^{-1})², with strongly time-dependent effects. In contrast, we observe no time-dependent effects when the interaction becomes strong (≥ 0.6 eV).

Over the last four decades, oxygen defective ceria has been widely used in multiscale applications from electrochemical devices to automotive catalysts, gas sensors, *etc.*^{1–3} Furthermore, a recent discovery demonstrated that ceria thin films display an unconventional electromechanical strain at room temperature.^{4–7} For example, the reported electrostriction coefficient (M_e) is around 6.5×10^{-18} (m V^{-1})² for $[\text{V}_\text{O}^\bullet\bullet] = 5\%$, *i.e.* 20 mol% Gd-doped ceria (GDC).⁴ Such a value is extremely high for a material with low dielectric constant ($\epsilon_r^{\text{GDC}} \approx 30$)⁸ and high elastic modulus ($Y^{\text{GDC}} \approx 200$ MPa).⁹ Surprisingly, in contrast to conventional inorganic ceramic materials, ceria thin films expand perpendicularly to the applied field direction. These properties are also investigated in bulk ceria and other oxygen defective fluorites ($\text{Bi}_2\text{O}_{3-\delta}$), illustrating similar outcomes.^{10–15} The atomistic origin of this uncommon behavior is associated with the presence of charge compensating oxygen vacancies ($\text{V}_\text{O}^\bullet\bullet$) in the ceria lattice.^{16,17} The $\text{V}_\text{O}^\bullet\bullet$ creates an electroactive elastic dipole ($\text{Ce}_{\text{Ce}}-\text{V}_\text{O}^\bullet\bullet$) having a long bond

Electromechanical dopant–defect interaction in acceptor-doped ceria†

Ahsanul Kabir,^{ib}*^a Victor Buratto Tinti,^a Maxim Varenik,^b Igor Lubomirsky^{ib}^b and Vincenzo Esposito^{ib}*^a

length and six anomalous reduced ($\text{Ce}_{\text{Ce}}-\text{O}_\text{O}$) bonds when compared to the bond length of undoped ceria, leading to the development asymmetric charge distribution and anisotropic local dipolar elastic field around the host lattice.¹⁸ Upon interaction with an electric field, this distorted fluorite lattice ($\text{Ce}_{\text{Ce}}\text{O}_\text{O}-\text{V}_\text{O}^\bullet\bullet$) complex becomes a more ideal-like fluorite structure and successively induces a considerable local strain and *vice versa*.^{16,17} Although governed by the $\text{Ce}_{\text{Ce}}-\text{V}_\text{O}^\bullet\bullet$ complex, the local configuration of an oxygen vacancy is a crucial feature controlling electrostriction in bulk ceria.^{16,19} Literature reports of both computational and experimental studies demonstrate that the configuration of oxygen vacancies in the lattice strongly depends on dopant size and valence, *i.e.*, electrostatic (attractive) and elastic (repulsive) interaction between the cation and vacancy.^{20–22} Fig. 1a schematically represents a simple configuration of dopant cations concerning nearby oxygen vacancies in a unit cell of ceria. In general, the acceptor dopant prefers to occupy the next neighbour (1nn) or next-nearest neighbour (2nn) lattice site of an oxygen vacancy. The electrostatic interaction favors the 1nn site while elastic

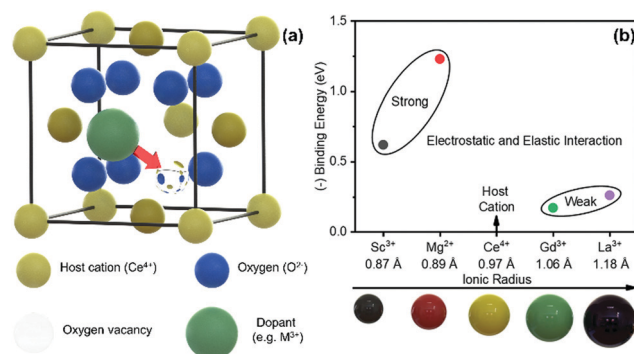


Fig. 1 (a) Schematic illustration of a unit cell of fluorite structured ceria, showing electrosteric interaction between the acceptor dopant and charge compensating oxygen vacancy. (b) Computationally calculated binding energy (1nn) values of variously doped ceria as a function of dopant radius. The data are taken from V. Butler *et al.*²⁴

^a Department of Energy Conversion and Storage, Technical University of Denmark, Kgs, Lyngby 2800, Denmark. E-mail: ahska@dtu.dk, vies@dtu.dk

^b Department of Materials and Interfaces, Weizmann Institute of Science, Rehovot 761001, Israel

† Electronic supplementary information (ESI) available. See DOI: 10.1039/d0ma00563k

Table 1 The estimated dielectric constant, relaxation frequency, and electrostriction coefficient of the samples at room temperature

Sample ID	$f_{g.b.}$ (Hz)	ϵ'	M_{33} (1 Hz) (m V^{-1}) ²	M_{33} (100 Hz) (m V^{-1}) ²
LDC	4.0×10^1	40	0.5×10^{-17}	0.04×10^{-17}
GDC	2.0×10^1	25	3.0×10^{-17}	0.15×10^{-17}
MDC	1.0×10^1	75	0.4×10^{-17}	0.25×10^{-17}
SDC	1.0×10^2	65	0.12×10^{-17}	0.15×10^{-17}

contribution (Fig. S4 and S5, ESI†). The resistivity of all compounds is strongly dominated by the grain boundary and they have an ion-blocking factor above 0.9 at 300 °C. The effect of the ion blocking property is qualitatively estimated by the parameter called grain boundary blocking factor ($\alpha_{g.b.}$), where

$$\alpha_{g.b.} = \frac{R_{g.b.}}{R_{bulk} + R_{g.b.}} \quad (19)$$

In cerium based oxides, not only grain boundary but also dopant-defect association, nanoclusters, dopant segregation, and residual pores all combined introduce the ion-blocking effect.^{2,28} The temperature-dependent total electrical conductivity (σ) is illustrated in Fig. 2b that follows the Arrhenius expression:

$$\sigma = \sigma_0 \exp\left(-\frac{E_a}{kT}\right) \quad (1)$$

where σ_0 is the pre-exponent factor and E_a the activation energy. Even though all samples contain equivalent oxygen vacancy concentration, the conductivity value differs significantly between the materials. The magnitude of conductivity increases with temperature showing a maximum for LDC and minimum for the SDC sample. Such outcomes simply emphasize the leading contribution of the oxygen vacancy configuration, *i.e.*, dielectric constant, dopant-defect interaction, and defect cluster on tuning the charge migration properties. We attribute the lowest conductivity value in SDC to its limited solubility in ceria, which is close to 3%.²⁹ Above the solubility level, it is highly expected that Sc^{3+} forms short- or long-range nanodomains in the lattice and/or grain boundaries. According to Nowick *et al.*, the Sc^{3+} dopant also acts as a scavenger for oxygen vacancies in cerium oxide.²⁹ Interestingly, the activation energy value is equivalent (~ 1.0 eV) in all samples, emphasizing that the mobility of oxygen vacancies is considerably different in each sample due to different dopant associated traps for vacancies.

The electrostrictive strain of the samples, with a response to the applied electric field, is illustrated in Fig. 3. As noticed, the strain starts to saturate at a particular electric field value, *e.g.*, $\sim 4\text{--}5$ kV cm^{-1} , for the LDC and GDC samples. The saturation of strain is fitted with the empirical equation:¹⁰

$$u(E^2) = M_{33} \cdot E_{\text{sat}}^2 \left[1 - \exp\left(-\frac{E^2}{E_{\text{sat}}^2}\right) \right] \quad (2)$$

here, M_{33} is the electrostriction strain coefficient, and E_{sat} is the saturation electric field. Above the saturation point, a further electrostrictive strain is no longer possible, since the elastic dipole comes to be fully aligned with the high electric field.¹⁵ Besides, at high frequencies, the strain value reduced significantly

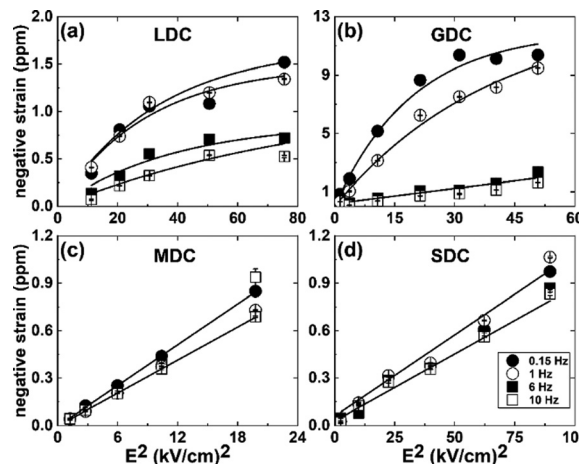


Fig. 3 (a–d) The negative electromechanical strain as a function of electric field square under applied frequencies from ~ 0.15 to 10 Hz.

but followed the typical linear relation.³⁰ On the other hand, neither strain saturation nor reduction was noticed for the SDC and MDC compounds. The electrostrictive strain coefficient (M_{33}) as a function of applied frequency is reported in Fig. 4a. As observed, the GDC illustrates maximum M_{33} value having one order higher magnitude in the low frequencies (≤ 2 Hz). At the low-frequency regime, for instance, below 10 Hz, the value of M_{33} for the GDC and LDC compound is strongly dependent on an applied frequency value. The M_{33} empirically follows a frequency-associated relaxation, given by:¹⁰

$$M_{33}(f) = \frac{M_{33}^0}{\sqrt{1 + (\tau f)^{2+\alpha}}} + M_{33}^\infty \quad (3)$$

where M_{33}^0 and M_{33}^∞ are the electrostriction coefficient value at low and high frequencies, respectively. τ is the characteristic relaxation time, and α is the non-ideality factor. The fitting parameters are illustrated in Table S1 (ESI†). Surprisingly, M_{33} does not obey such relation for the SDC and MDC samples. These materials display a frequency-independent steady M_{33} value of about $\sim 0.1\text{--}0.3 \times 10^{-17}$ (m V^{-1})². At a high-frequency region, *e.g.*, above 10 Hz, the GDC exhibits a similar M_{33} value to the former, while LDC displays an order smaller M_{33} of roughly 0.03×10^{-17} (m V^{-1})² (see Fig. 4b). Finally, the M_{33} value in the order of $\geq 0.1 \times 10^{-17}$ (m V^{-1})² is still one order of magnitude larger than the classical Newnham empirical law

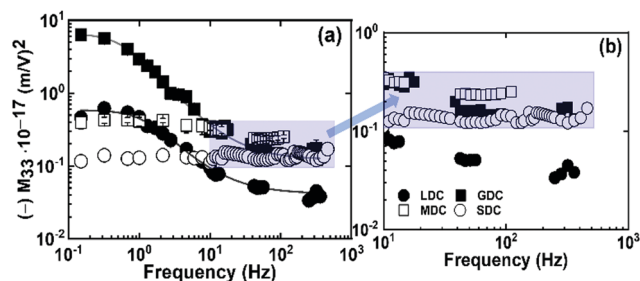


Fig. 4 Frequency-dependent electrostrictive strain coefficient (M_{33}) of all samples at (a) 0.15–700 Hz and (b) high-frequency regime.



